

Aging and equilibration in bistable contagion dynamics

Paul Richter,¹ Malte Henkel,^{2,3,4} and Lucas Böttcher^{5,1,6}

¹*Institute for Theoretical Physics, ETH Zurich, 8093, Zurich, Switzerland**

²*Laboratoire de Physique et Chimie Théoriques (CNRS UMR 7019),*

Université de Lorraine Nancy, B.P. 70239, F - 54506 Vandœuvre lès Nancy Cedex, France†

³*Centro de Física Teórica e Computacional, Universidade de Lisboa, P - 1749-016 Lisboa, Portugal*

⁴*MPIPKS, Nöthnitzer Straße 38, D - 01187 Dresden, Germany*

⁵*Computational Medicine, UCLA, 90024, Los Angeles, United States*

⁶*Center of Economic Research, ETH Zurich, 8092, Zurich, Switzerland‡*

(Dated: December 8, 2021)

The late-time relaxation dynamics is analyzed for a general contagion model. In this model, nodes are either active or failed. Active nodes can fail either “spontaneously” at any time or “externally” if their neighborhoods are sufficiently damaged. Failed nodes may always recover spontaneously. At late times, the breaking of time-translation-invariance is a necessary condition for physical aging. Indeed, we observe that time-translational invariance is lost for initial conditions that lie between the basins of attraction of the model’s two stable stationary states. Based on corresponding mean-field predictions, we characterize the observed model behavior in terms of a phase diagram spanned by the fractions of spontaneously and externally failed nodes. For the square lattice, the phases in which the dynamics approaches one of the two stable stationary states are not linearly separable due to spatial correlation effects. Our results provide new insights into aging and relaxation phenomena that are observable in a model of general contagion processes.

I. INTRODUCTION

The study of dynamical processes in complex systems is relevant in various contexts and contributed to a better understanding of the spreading of epidemics [1–6], opinions [7], innovations [8], and other contagious phenomena. Seemingly different models that have been developed to describe the aforementioned processes share various (universal) properties. For some models, it is possible to observe such universal features in their relaxation dynamics. This behavior is also known as *physical aging* and defined by (i) non-exponential, slow relaxation, (ii) breaking of time-translation invariance, and (iii) dynamical scaling [9]. Examples of systems with a non-equilibrium steady state that exhibit aging include directed percolation [10–12], population dynamics [13], and gel-forming polymers [14].

Identifying universal dynamical features in non-equilibrium systems may be useful to make predictions about their behavior and, in the case of contagious processes, develop control and intervention protocols. Here we focus on the aging characteristics of a general contagion model that captures a variety of simple (i.e., single contact) and complex (i.e., multiple contact) contagion dynamics [15, 16] in terms of spontaneous and externally-induced infection/failure processes. Models of simple contagions are common tools to describe the spread of epidemics [1]. In contrast to simple contagions where one infected individual is able to infect others, complex contagions require contact with multiple “infected” individ-

uals [17, 18]. Examples of complex contagions include the diffusion of innovations [8, 19], political mobilization [20], viral marketing [21], and coordination games [22].

Previous studies [10–12] investigated the aging properties of simple contagions whose phase space consists of an absorbing and a fluctuating phase with unique stationary states. Within these two phases, relaxation is exponential whereas slow (algebraic) relaxation can be observed at the critical point where the two phases merge [9]. For complex contagions, the phase space cannot be described by two phases with unique stationary states. Instead, it is characterized by a bistable regime [15, 16, 23] that gives rise to relaxation towards one of two stable stationary states.

In this work, we study relaxation and aging kinetics of complex contagions within their bistable region. In Sec. II, we introduce the general contagion model and provide an overview of corresponding mean-field results and concepts from the study of aging. In Sec. III, we numerically determine a phase portrait of bistable contagion dynamics on a square lattice and study the influence of different initial densities of failed nodes on the relaxation characteristics. To provide more insights into the relaxation properties, we map the observed dynamics to a phase diagram spanned by the fractions of spontaneously and externally failed nodes in Sec. IV. We find that the dynamics is initially driven by spontaneous transitions and approaches a line along which externally-induced transitions drive the system to one of the two stable stationary states. We conclude our study and discuss our results in Sec. VI.

* richterp@ethz.ch

† malte.henkel@univ-lorraine.fr

‡ lucasb@ethz.ch

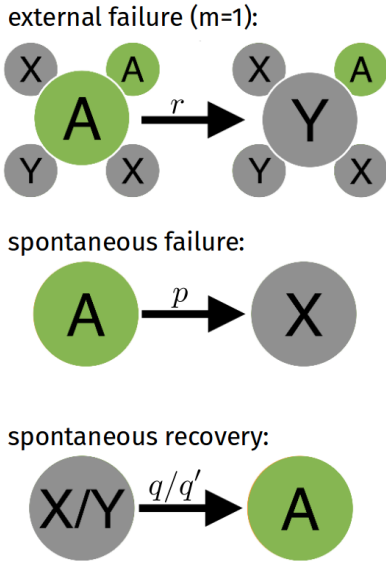


FIG. 1. **Schematic of model dynamics.** Nodes are arranged in a square lattice. Active nodes (A) can fail spontaneously (spontaneous failure) with rate p or if their neighborhoods are sufficiently damaged (external failure) with rate r . The corresponding recovery rates are q and q' . We use X and Y to indicate that nodes failed spontaneously and externally, respectively. A node fails externally if less than or equal to m of its neighbors are active.

II. MODEL AND METHODS

We consider a general contagion model on a network whose N nodes are either active (A) or failed (X or Y) [15, 16]. Active nodes can fail “spontaneously” with rate p or “externally” with rate r if their neighborhoods are sufficiently damaged. We use X and Y to denote the state of nodes that failed spontaneously and externally, respectively. External failure occurs if the number of active nearest neighbors of a node is smaller than or equal to the threshold m . Failed nodes in states X and Y recover with rates q and q' , respectively. We illustrate the described failure and recovery processes in Fig. 1.

To formulate the corresponding mean-field rate equations, let $n(t) \in [0, 1]$ be the fraction of active nodes, which is one minus the sum of the fractions of nodes $u(t)$ and $v(t)$ that failed spontaneously and externally (i.e., $n(t) + u(t) + v(t) = 1$). We use n_{st} to denote the total fraction of active nodes in the stationary state. For the derivation of the mean-field rate equations, we assume perfect mixing and first focus on the spontaneous-failure dynamics:

$$\frac{du(t)}{dt} = pn(t) - qu(t), \quad (1)$$

where the first term accounts for spontaneous failure with rate p and the second term accounts for spontaneous recovery with rate q .

We use the term *critically-damaged neighborhood* (CDN) to refer to a neighborhood where the number of active neighbors is smaller than or equal to m . The probability that a node of degree k is located in a CDN is $E_k = \sum_{j=0}^m \binom{k}{k-j} (1-n)^{k-j} n^j$. Therefore, the time evolution of externally-failed nodes is given by:

$$\frac{dv(t)}{dt} = r \sum_k f_k E_k n(t) - q'v(t), \quad (2)$$

where f_k is the degree distribution. The first term describes that active nodes become inactive with rate r if their neighborhood contains a sufficient number of inactive ones and the second term accounts for spontaneous recovery of these nodes with rate q' . For regular networks with degree k , a hysteresis region exists for $m < k - 1$ [15, 16]. Within this region, there are three stationary states with densities of active nodes n_{st}^1 , n_{st}^2 , and n_{st}^3 . The stable stationary states have densities n_{st}^1 and n_{st}^3 and the density of the unstable state is n_{st}^2 . We shall outline in Sec. IV that the unstable stationary state is best characterized by the corresponding densities of externally and spontaneously failed nodes (u_{st}^2 , v_{st}^2).

All numerical mean-field solutions are based on an explicit Euler forward integration scheme with time step $\Delta t = 0.01$. To simulate the described reactions on a square lattice of linear dimension L and with $N = L \times L$ nodes, we use kinetic Monte-Carlo (i.e., Gillespie) methods [24, 25]. At time t , each node $i \in \{1, 2, \dots, N\}$ is either active or failed. In our simulations, we keep track spontaneously and externally failed nodes and indicate the failure of node i at time t by $n_i(t) = 0$. Similarly, we indicate an active state of node i at time t by $n_i(t) = 1$.

To compare the relaxation properties that result from initial conditions close to the stable and unstable states, we quantify the relaxation dynamics of the described contagion model in terms of the autocorrelation function Γ and autocovariance function C :

$$\Gamma(t, s) = \langle n_i(t)n_i(s) \rangle, \quad (3)$$

$$C(t, s) = \langle n_i(t)n_i(s) \rangle - \langle n_i(t) \rangle \langle n_i(s) \rangle, \quad (4)$$

where angular brackets $\langle \cdot \rangle$ denote an ensemble average. In systems that exhibit aging, both Γ and C do not depend on $t - s$ alone, but are also expected to obey the following scaling behavior [9, 12]:

$$\Gamma(t, s) = s^{-b} f_{\Gamma}(t/s), \quad f_{\Gamma}(y) \sim y^{-\lambda_{\Gamma}/z}, \quad (5)$$

$$C(t, s) = s^{-b} f_C(t/s), \quad f_C(y) \sim y^{-\lambda_C/z}, \quad (6)$$

for $t, s \gg \tau_{\text{micro}}$ and $t - s \gg \tau_{\text{micro}}$, where τ_{micro} is a microscopic reference time scale. The exponent z is the dynamical exponent and the autocorrelation exponents λ_{Γ} and λ_C are defined from the asymptotics for $y = t/s \gg 1$ of the corresponding scaling functions.

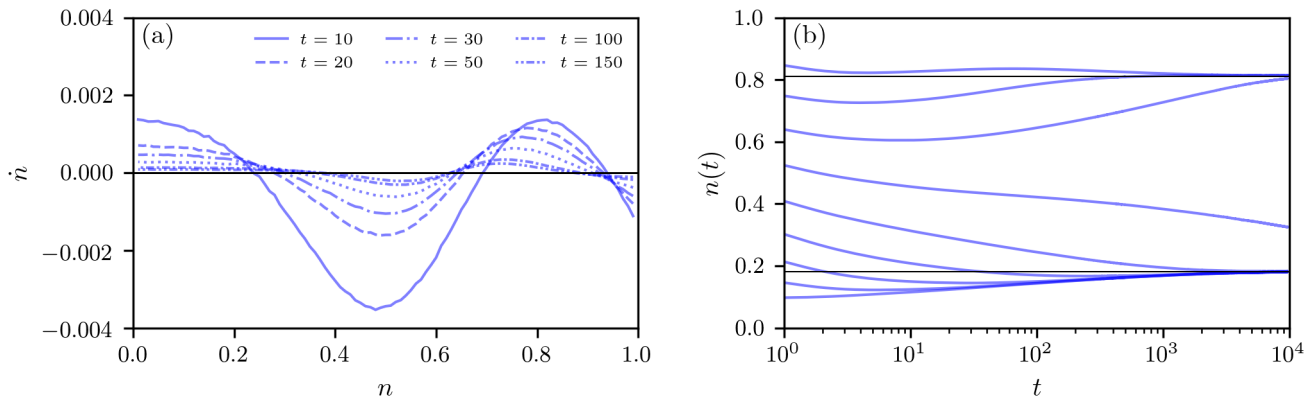


FIG. 2. **Phase portrait and relaxation dynamics.** (a) The numerically-determined phase portrait of the general contagion model for $m = 1$, $r = 0.95$, $p = 1.0$, $q = 1.0$, and $q' = 0.1$ of the fraction of active nodes $n(t)$ for different times t . Simulations were performed on a square lattice with $N = 512 \times 512$ sites using 10^3 samples for each data point. (b) The time evolution of $n(t)$ for different initial conditions on a square lattice with $N = 1024 \times 1024$ sites. We use the following initial densities of active nodes: $n(0) = [0.1, 0.2, \dots, 0.9]$. In all simulations, we set the initial density of spontaneously-failed nodes to zero and use uniformly distributed externally-failed nodes such that the initial density of active nodes satisfies $n(0) = 1 - v(0)$.

III. RELAXATION DYNAMICS

The general contagion model exhibits a bistable regime for certain thresholds and failure and recovery rates [15, 16]. One possible choice is to set $m = 1$, $r = 0.95$, $p = 1.0$, $q = 1.0$, and $q' = 0.1$ to obtain bistable dynamics on a square lattice. We use these parameters for our simulations on the square lattice throughout the manuscript. Initially, we set the density of spontaneously-failed nodes to zero and use uniformly distributed externally-failed nodes. The initial density of active nodes is thus $n(0) = 1 - v(0)$. Since we are interested in the relaxation properties of the model dynamics within this bistable region, we first determine the initial density of active nodes $n^*(0)$ from which the system eventually relaxes into one of the two stable stationary states with densities n_{st}^1 and n_{st}^3 . Mathematically, $n^*(0)$ is the separatrix in the initial density $n(0)$ such that for $n(0) > n^*(0)$, the system evolves toward the steady state with density n_{st}^1 and for $n^*(0) < n(0)$, the system evolves towards the steady state with density n_{st}^3 . Note that $n^*(0)$ is not the same as the density of active nodes in the unstable density of states (see Sec. IV).

After initializing the dynamics, we numerically construct a phase portrait of $n(t)$ by approximating the slope \dot{n} in terms of the finite-difference derivative $(n(t + \Delta t) - n(t))/\Delta t$ with $\Delta t = 0.1t$. Based on the behavior of \dot{n} in Fig. 2(a), we can identify all stationary states (i.e., the states for which the density of active nodes satisfies $\dot{n} = 0$). Close to the initial density of active nodes $n^*(0)$, the slope \dot{n} changes its sign from negative to positive values and we conclude that $n \approx 0.62 = n^*(0)$. To determine the densities of the two stable stationary states, we perform corresponding simulations on a square lattice with 1024×1024 nodes. In Fig. 2(b), we show the cor-

responding time evolution of the density of active nodes $n(t)$ for different initial conditions. For the considered failure rates, we find that the densities of active nodes in the two stable stationary state are $n_{st}^1 \approx 0.18$ and $n_{st}^3 \approx 0.81$.

The numerically-obtained phase portrait of the square lattice is qualitatively very similar to corresponding mean-field results [16]. However, in the following sections, we show that spatial correlation effects on the square lattice lead to subtle deviations of the initial relaxation dynamics from mean-field predictions. In Fig. 3, we provide a more detailed picture of the relaxation dynamics in the vicinity of $n^*(0)$. If the initial fraction of active nodes is larger than $n^*(0) \approx 0.62$, the curves move towards the upper stable stationary states; for initial fractions below $n^*(0)$ they approach the lower point of stability. The closer the initial density is to $n^*(0) \approx 0.62$, the slower it approaches one of the stable stationary states. This behavior can also be understood in terms of the phase portrait in Fig. 2(a). If the system is sufficiently close to the $n^*(0)$, the slope \dot{n} approaches zero.

The slow relaxation dynamics in systems that exhibit aging is mathematically often described by a power law $n(t) \sim t^{-\delta}$ and we find $\delta \approx 0$ for the equilibration behavior close to the unstable stationary state. We observe in Fig. 2(b) that the fraction of active nodes may first decrease and then increase again for certain initial conditions. In the next section, we further investigate this behavior by illustrating the system's time evolution in terms of a phase diagram spanned by the fractions of spontaneously and externally-failed nodes.

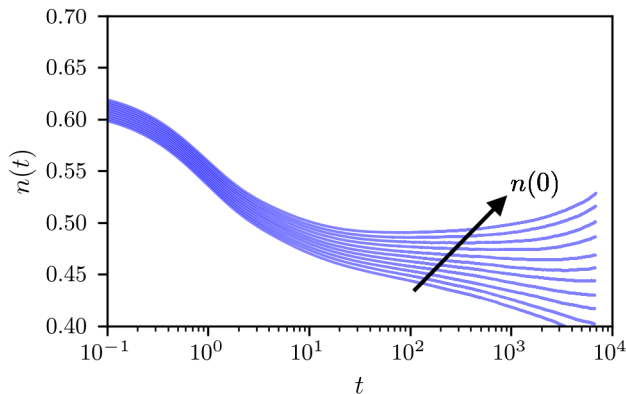


FIG. 3. **Relaxation in the vicinity of the unstable stationary state.** We show the relaxation dynamics of the general contagion model for $m = 1$, $r = 0.95$, $p = 1.0$, $q = 1.0$, and $q' = 0.1$ on a square lattice with $N = 1024 \times 1024$ nodes. The chosen initial densities are close to $n^*(0) \approx 0.62$. For initial densities $n(0) > n_{st}^2$, we observe that $n(t)$ moves towards the upper stationary state, while for $n(0) < n_{st}^2$ the densities move towards the lower stationary state. We used the following initial densities: $n(0) = [0.610, 0.612, 0.614, \dots, 0.630]$. Since the time axis begins at $t = 10^{-1}$ and not at $t = 0$, the densities have already decreased slightly.

IV. PHASE DIAGRAM

To better understand the initial relaxation dynamics, we study the evolution of the density of active nodes in the $u-v$ plane. In Fig. 4(a), we show the evolution of the densities $u(t)$ and $v(t)$ for different initial conditions on a square lattice. We observe that the evolution of all trajectories can be divided into two stages I and II. During stage I, the evolution of a trajectory is mainly driven by spontaneous-failure dynamics. After some time, all trajectories approach an “equilibration line” and relax towards one of the two stable stationary states (stage II). The relaxation during stage I is much faster than the relaxation in stage II (see inset in Fig. 4 (a)). We find the following densities of spontaneously- and externally-failed nodes at the two stable stationary states

$$\begin{aligned} u_{st}^1 &= 0.019(1) & \text{and} & & v_{st}^1 &= 0.803(1), \\ u_{st}^3 &= 0.087(1) & \text{and} & & v_{st}^3 &= 0.100(1). \end{aligned} \quad (7)$$

Note that the corresponding densities of active nodes $n_{st}^1 = 1 - u_{st}^1 - v_{st}^1 = 0.178(1)$ and $n_{st}^3 = 1 - u_{st}^3 - v_{st}^3 = 0.813(1)$ are equal to the values that we reported in Sec. III. Although the stable stationary states with densities n_{st}^1 and n_{st}^3 can be identified with the phase portrait and evolution plots of $n(t)$ (see Fig. 2), the situation is more complex for the characterization of the unstable stationary state.

In our simulations, we set $u(0) = 0$ and use uniformly-distributed externally failed nodes for the simulations in Figs. 2 and 3. The actual unstable point lies at

$(u_{st}^2, v_{st}^2) = (0.060(5), 0.370(10))$ and has a density of active nodes $n_{st}^2 = 0.570(15)$. The point $n^*(0)$ (i.e., $(u(0), v(0)) = (0, 0.38)$) of Sec. III lies at the boundary that separates the phases in which they dynamics either approaches the upper or the lower stable stationary state.

On the square lattice, we find additional effects that make the dynamics even more complex. We observe in Fig. 4(a) that the evolution of $u(t)$ and $v(t)$ is not fully determined by these two densities alone. For $(u, v) \approx (0.3, 0.3)$, the blue trajectory starting at $(u(0), v(0)) = (0.6, 0.2)$ and ending at (u_{st}^3, v_{st}^3) intersects with the orange trajectory, which converges towards $(u_{st}^1, v_{st}^1) = (0.019, 0.803)$. Based on this result, we conclude that the evolution of $(u(t), v(t))$ on a square lattice depends on the initial densities $(u(0), v(0))$ even if two trajectories share the same densities at some time. In other words, it is not possible to describe the observed dynamics on a square lattice in terms of differential equations of $u(t)$ and $v(t)$. The described effect can be also understood in terms of the fractions of CDNs, as we show in Fig. 4(c). Initially, we distribute all externally-failed nodes uniformly at random on the lattice. The corresponding initial density of CDNs is $CDN(0) \approx 0.13$. At time $t \approx 0.77$, the aforementioned blue and orange trajectories intersect. At this time, the density of CDNs of the blue trajectory is $CDN(0.77) \approx 0.1$, whereas the (initial) density of CDNs of the orange trajectory is $CDN(0.77) \approx 0.2$.

For a qualitative comparison, we solve the mean-field rate equations of $u(t)$ and $v(t)$ (see Eqs. (1) and (2)) for parameters that lead to a bistable contagion dynamics. We show the corresponding $u-v$ phase space in Fig. 4 (b). Similar to the observation that we made for the square-lattice case, the inset in Fig. 4 (b) shows that the relaxation of the spontaneous-failure dynamics is faster than the induced-failure dynamics. This mean-field analysis also enables us to identify two distinct phases. All trajectories that originate within the blue region approach the stable stationary state with density n_{st}^3 . The remaining trajectories that originate in the orange region move towards the second stable stationary state density n_{st}^1 . Unlike in the square-lattice phase space, both phases can be linearly separated, because the mean-field system is fully determined by the densities $u(t)$ and $v(t)$ since the mean-field dynamics is described by deterministic differential equations (see Eqs. (1) and (2)) with unique trajectories. Thus, if two trajectories share the same value of $u(t)$ and $v(t)$, they also have the same fractions of CDNs (see Fig. 4(d)).

V. CORRELATION EFFECTS

In Secs. III and IV, we outlined the influence of different initial conditions on the relaxation characteristics of the general contagion model. We initialize the dynamics with $n(0) = 0.62 \approx n^*(0)$ and $n(0) = 0.81 \approx n_{st}^3$. The corresponding initial densities of spontaneously and externally failed nodes are $(u(0), v(0)) = (0, 0.38)$ and

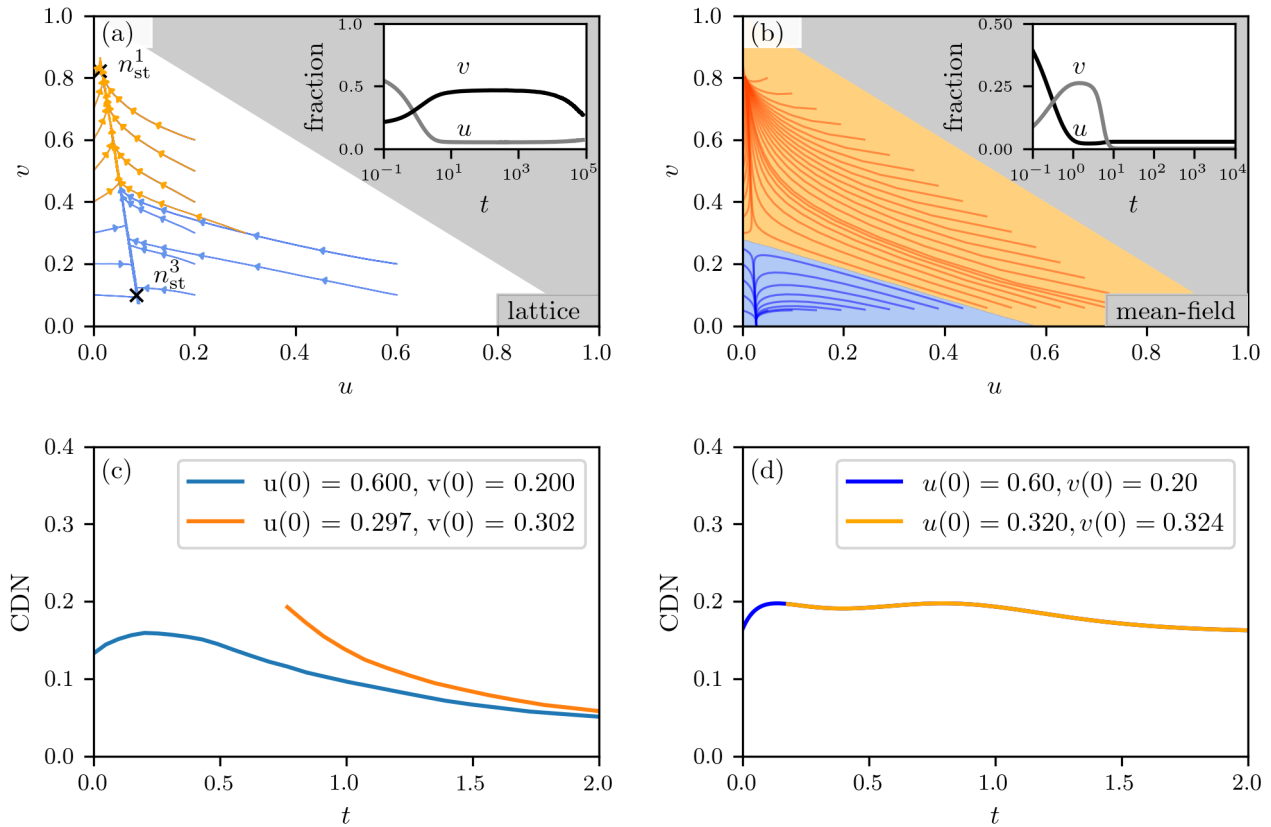


FIG. 4. **Relaxation for different fractions of externally and internally failed nodes.** (a) The relaxation of the model dynamics in the $u-v$ plane for different initial conditions. All trajectories first approach an “equilibration line” (stage I) and then slowly relax towards one of the two stable stationary states that we indicate by black crosses (stage II). Blue and orange trajectories approach the stationary states with densities n_{st}^1 and n_{st}^3 , respectively. Simulations were performed on a square lattice with $N = 1024 \times 1024$ nodes and for parameters $m = 1$, $r = 0.95$, $p = 1.0$, $q = 1.0$, and $q' = 0.1$. (b) Corresponding mean-field trajectories (black solid lines) in the $u-v$ plane for different initial conditions and $m = 1$, $r = 5.0$, $p = 0.1$, $q = 3.5$, and $q' = 1.0$. Within the orange (blue) region, all trajectories approach the stationary state with density n_{st}^1 (n_{st}^3). To obtain the mean-field trajectories, we numerically solved Eqs. (1) and (2). In both panels, grey-shaded regions correspond to densities $n > 1$ and are excluded from our analysis. (c) The fractions of CDNs for the two trajectories that cross in (a). For initial conditions $(u(0), v(0)) = (0.6, 0.2)$ (blue solid line), we observe that the proportions of CDNs are smaller than for $(u(0.77), v(0.77)) \approx (0.3, 0.3)$. (d) If two mean-field trajectories share the same densities u and v , they converge towards the same stationary state.

$(u(0), v(0)) = (0, 0.19)$. We now analyze the relaxation properties of the general contagion dynamics for such initial densities. We use a 512×512 square lattice and generate 10^3 samples. Based on these samples, we compute the autocorrelation function C and autocovariance function Γ (see Eqs. (3) and (4)).

In Fig. 5, we show $\Gamma(T+t, s)$ and $C(T+t, s)$ as functions of $t-s$ for different values of T and s . In Fig. 5(a-b), the initial density $n(0) = 0.62 \simeq n^*(0)$ and we observe that both correlation functions are not time-translational invariant as we cannot obtain a data collapse when plotting $\Gamma(t, s)$ and $C(t, s)$ as a function of $t-s$. During the initial fast relaxation, close to the stable stationary state with density $n_{st}^3 \approx 0.81$, we find that $\Gamma(t, s) = \langle n_i(t)n_i(s) \rangle$ becomes stationary since the dynamics approaches the stable stationary state exponen-

tially fast (see Fig. 5(c)). Comparing Figs. 5(b) and (d) shows that the dependence of the autocovariance function $C(t, s)$ on s is less pronounced for an initial density close to n_{st}^3 than for $n^*(0)$. However, if we let the dynamics evolve for a period $T = 5000$ before determining the correlation functions, we find that $\Gamma(t, s)$ and $C(t, s)$ become time-translational invariant for both considered initial conditions (see Figs. 5(f-h)). The trajectory that started close to the stable stationary state fluctuates around n_{st}^3 and the trajectory that started at $n(0) = 0.62$ either approached one of the stable stationary states or is still located between the basins of attraction of the two stable stationary states (see Fig. 3).

In Fig. 6, we show $C(T+t, T+s)$ for different initial relaxation times $T \in \{0, 100, 500, 1000, 2000, 5000\}$. We account for the additional T -dependence in Eq. (4) and

obtain

$$C(T+t, T+s) = (T+s)^{-b} f_C((T+t)/(T+s)). \quad (8)$$

If $s \ll T$ and $T \ll t$, we can expand the argument of f_C as follows:

$$\frac{T+t}{T+s} = 1 + \frac{t-s}{T} + \frac{ts}{T^2} \sim 1 + \frac{t-s}{T}. \quad (9)$$

The resulting autocovariance function is (see Eq. (6))

$$C(T+t, T+s) \sim T^{-b} (1 + (t-s)/T)^{-\lambda_C/z}. \quad (10)$$

We have thus shown that the function $C(T+t, T+s)$ only depends on $t-s$ for large values of T (see Figs. 5(e-h)). This result is in agreement with the data that we show in Fig. 6. For $T = 500, 1000, 2000$, and 5000 , we observe that $C(T+t, T+s)$ is well-captured by a function of $t-s$.

For the described initialization protocol, we would expect that $n(t) \propto t^{-\delta}$ with $\delta \approx 0$ for initial densities $n(0)$ close to the density $n^*(0)$. We observe in Fig. 7(a) that the exponent λ_Γ/z of Eq. (5) satisfies the relation $\lambda_\Gamma/z = \delta \approx 0$ that was found in other systems exhibiting aging [9, 12]. For the autocovariance function $C(t, s)$, we observe a data collapse when, according to Eq. (6), plotted as function of $s^{-b} f_C(t/s)$, confirming the relation $b = 2\delta \approx 0$ [9, 12]. The corresponding scaling exponent is $\lambda_C/z = 2.1(1)$ (see Fig. 7(b)). This is not too different from the estimate $\lambda_C/z = 2.8(3)$ of the 2D contact process [10–12] but not accurate enough for a quantitative comparison.

VI. CONCLUSIONS AND DISCUSSION

We have studied the relaxation properties of a general contagion model that describes simple (i.e., single contact) and complex (i.e., multiple contact) contagion phenomena. Relaxation and aging properties of simple contagions or contact processes have been analyzed in previous works [10–12]. Here we analyzed the relaxation and

aging dynamics of complex contagion phenomena within their bistable region [15, 16].

Our numerical analyses of the relaxation behavior of complex contagion dynamics show that the phase portrait and large parts of the relaxation dynamics are qualitatively captured by corresponding mean-field results [16]. However, our results also indicate that the phase space of the considered general contagion model is more complex than previously realized [15, 16, 23] since it cannot be solely described by the density of failed nodes. For complex contagion dynamics on a square lattice, we have also shown that the phases in which the dynamics approach either the upper or lower stable stationary states are not linearly separable. Trajectories that cross in (u, v) space at a certain time may approach different stationary states due to the influence of structural effects in the initial conditions. Aging effects can be observed for initial conditions that are close to the boundary that separates the phases in which the dynamics approach one or the other stationary state. The observed relaxation exponent δ is almost zero and the resulting aging phenomena are similar to those observed for the spherical model in an external magnetic field [26]. Since the universality class of the 2D SIR model is thought to be the same as the one of dynamical percolation [6], it would be desirable to dispose direct studies of aging in this universality class.

ACKNOWLEDGMENTS

LB acknowledges financial support from the SNF Early Postdoc.Mobility fellowship on “Multispecies interacting stochastic systems in biology” and the Army Research Office (W911NF-18-1-0345). All simulations have been performed on the ETH Euler cluster.

-
- [1] M. J. Keeling and P. Rohani, *Modeling Infectious Diseases in Humans and Animals* (Princeton University Press, 2008).
 - [2] L. Böttcher, O. Woolley-Meza, N. A. M. Araújo, H. J. Herrmann, and D. Helbing, *Sci. Rep.* **5**, 16571 (2015).
 - [3] R. Pastor-Satorras, C. Castellano, P. V. Mieghem, and A. Vespignani, *Rev. Mod. Phys.* **87** (2015).
 - [4] L. Böttcher, O. Woolley-Meza, E. Goles, D. Helbing, and H. J. Herrmann, *Phys. Rev. E* **93**, 042315 (2016).
 - [5] J. Dehning, J. Zierenberg, F. P. Spitzner, M. Wibral, J. P. Neto, M. Wilczek, and V. Priesemann, *Science* (2020).
 - [6] T. Tomé and R. M. Ziff, *Phys. Rev. E* **82**, 051921 (2010).
 - [7] A. Flache, M. Mäs, T. Feliciani, E. Chattoe-Brown, G. Deffuant, S. Huet, and J. Lorenz, *Journal of Artificial Societies and Social Simulation* **20** (2017).
 - [8] E. M. Rogers, *Diffusion of Innovations* (Simon and Schuster, New York, 2003).
 - [9] M. Henkel and M. Pleimling, *Non-Equilibrium Phase Transitions: Volume 2: Ageing and Dynamical Scaling Far from Equilibrium* (Springer Science & Business Media, 2011).
 - [10] T. Enss, M. Henkel, A. Picone, and U. Schollwöck, *J. Phys. A* **37**, 10479 (2004).
 - [11] J. J. Ramasco, M. Henkel, M. A. Santos, and C. A. da Silva Santos, *J. Phys. A* **37**, 10497 (2004).
 - [12] L. Böttcher, H. J. Herrmann, and M. Henkel, *J. Phys. A* **51**, 125003 (2018).
 - [13] S. Chen and U. C. Täuber, *Phys. Biol.* **13**, 025005 (2016).

- [14] M. Kohl, R. Capellmann, M. Laurati, S. Egelhaaf, and M. Schmiedeberg, *Nat. Comm.* **7**, 11817 (2016).
- [15] L. Böttcher, M. Luković, J. Nagler, S. Havlin, and H. J. Herrmann, *Sci. Rep.* **7**, 41729 (2017).
- [16] L. Böttcher, J. Nagler, and H. J. Herrmann, *Phys. Rev. Lett.* **118**, 088301 (2017).
- [17] M. Granovetter, *Am. J. Sociol.* **83**, 1420 (1978).
- [18] D. Centola and M. Macy, *Am. J. Sociol.* **113**, 702 (2007).
- [19] J. Coleman, E. Katz, and H. Menzel, *Sociometry* **20**, 253 (1957).
- [20] M. S. Chwe, *Am. J. Sociol.* **105**, 128 (1999).
- [21] J. Leskovec, L. A. Adamic, and B. A. Huberman, *ACM Trans. Web* **1** (2007).
- [22] D. Easley and J. Kleinberg, *Networks, crowds, and markets: Reasoning about a highly connected world* (Cambridge University Press, 2010).
- [23] A. Majdandzic, B. Podobnik, S. V. Buldyrev, D. Y. Kenett, S. Havlin, and H. E. Stanley, *Nat. Phys.* **10**, 34 (2014).
- [24] D. T. Gillespie, *J. Comput. Phys.* **22**, 403 (1976).
- [25] D. T. Gillespie, *J. Phys. Chem.* **81**, 2340 (1977).
- [26] M. Paessens and M. Henkel, *J. Phys. A* **36**, 8983 (2003).

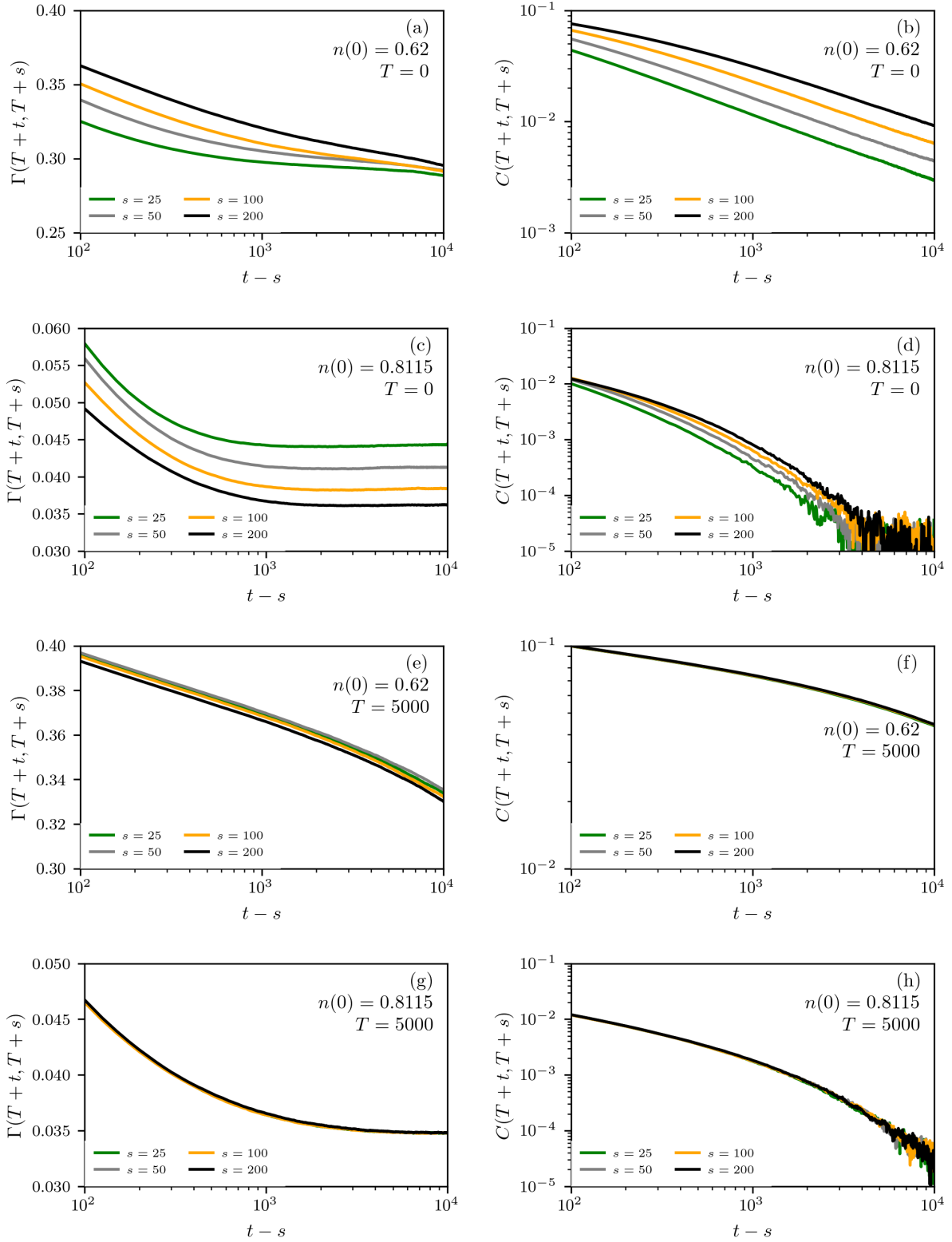


FIG. 5. **Correlation and covariance functions for different densities of active nodes.** We show the correlation function $\Gamma(t, s)$ and covariance function $C(t, s)$ (see Eqs. (3) and (4)) as functions of $t - s$. In panels (a–d), we show $\Gamma(t, s)$ and $C(t, s)$ without an initial relaxation period (i.e., $T = 0$). For a comparison with longer initial relaxation times, we set $T = 5000$ in panels (e–h). In panels (c–d) and (g–h), we use an initial condition of $n(0) = 0.8115$ (close to the upper stationary state) and we set $n(0) = 0.62 = n^*(0)$ in panels (a–b) and (e–f). In our simulations, we used a square lattice with $N = 512 \times 512$ sites and generated 1000 samples. As we show in panel (g), the correlation function Γ converges towards the square of the density n_{st}^3 with the value $(1 - n_{st}^3)^2 \approx 0.035$.

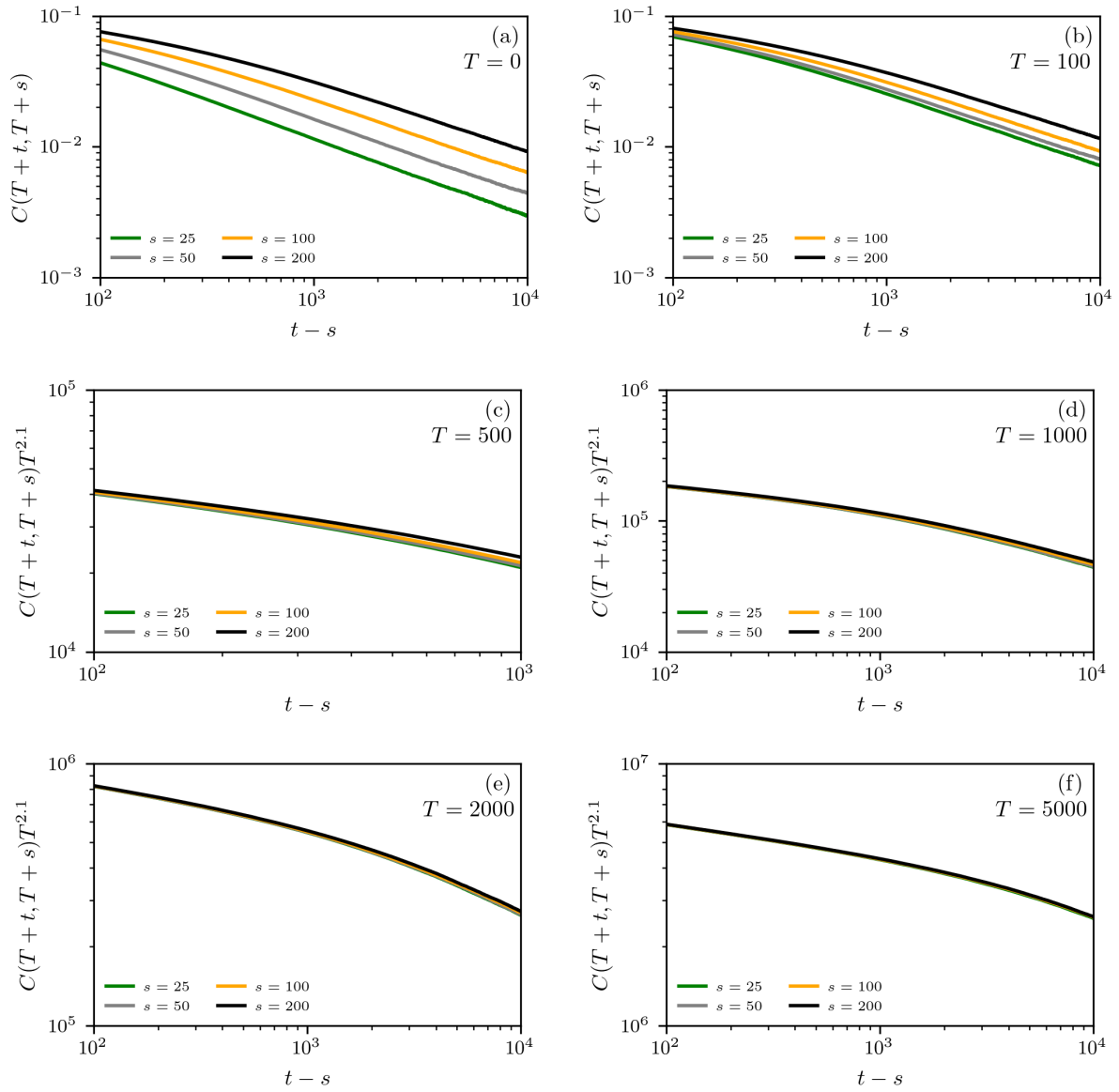


FIG. 6. **Covariance functions at $n^*(0)$ for different relaxation times.** We show the covariance function $C(T+t, T+s)$ (see Eq (4)) as a function of $t-s$. We use an initial density of $n(0) = 0.62 = n^*(0)$ and let the system relax for a period T before measuring the correlation functions. The relaxation times were chosen as $T = 0$ (a), $T = 100$ (b), $T = 500$ (c), $T = 1000$ (d), $T = 2000$ (e), and $T = 5000$ (f). In our simulations, we use a square lattice with $N = 512 \times 512$ sites and generated 1000 samples for each value T .

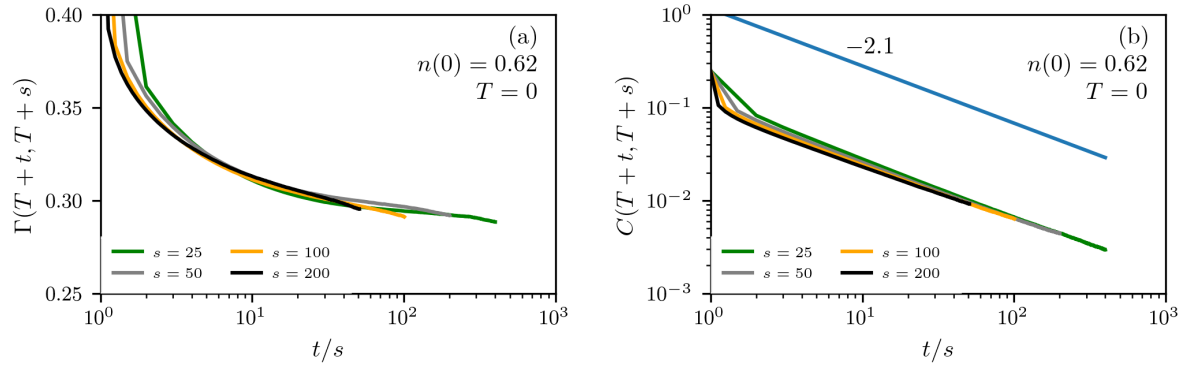


FIG. 7. **Correlation and covariance functions at $n^*(0)$.** We show the correlation function $\Gamma(t, s)$ and $C(t, s)$ (see Eqs. (3) and (4)) as functions of t/s . In both panels (a) and (b), we use an initial density of $n(0) = 0.62 = n^*(0)$. All simulations were performed on a square lattice with $N = 512 \times 512$ sites and without any initial relaxation before measuring the correlation functions (i.e., $T = 0$). The number of samples is 1000.